Sparse Signal Reconstruction using Variational Methods with Fractional Derivatives

Stefan Stojanović*, Thomas Debarre†, Michael Unser†

***Abstract*—In this paper we investigate the use of generalized (γ, τ)-fractional derivatives as regularization operators in inverse problems. We focus on reconstructing periodic signals which are sparse in the continuous-domain by using generalized total-variation (gTV). We use the periodic B-splines basis for the signal representation, which enables us to recast the continuous optimization problem as a finite-dimensional one in an exact way. We investigate the optimality of our algorithm for the reconstruction of self-similar stochastic processes, and we validate experimentally the superiority of gTV over Tikhonov L_2 regularization for sparse α-stable self-similar processes.**

***Index Terms*—fractional splines, total variation, sparsity, periodic splines, self-similar stochastic processes**

I. Introduction

A. Continuous-domain inverse problems

In this work we focus on reconstructing a continuous signal f_0 using M noisy measurements $\mathbf{y} \in \mathbb{R}^M$ which are acquired through a continuous forward model $\boldsymbol{\nu}$ so that $\boldsymbol{\nu}(f_0) \approx \mathbf{y}$. The reconstructed signal f should conform with the noisy measurements. A classical reconstruction method consists in minimizing an objective functional which includes the difference between the forward model applied to the reconstructed signal $\boldsymbol{\nu}(f) \in \mathbb{R}^M$ and the measurements $\mathbf{y}$. This results in a data-fidelity term in the objective functional (typically a quadratic loss). In order to promote prior knowledge on the form of the signal and to reduce the ill-posedness of the problem, a regularization term $\mathcal{R}(f)$ is typically added to the objective functional. The reconstructed signal is a solution of the optimization problem given by:

$$\min_f ||\boldsymbol{\nu}(f) - \boldsymbol{y}||_2^2 + \lambda \mathcal{R}(f), \tag{1}$$

where $\lambda \geq 0$ is a regularization parameter. Higher values of λ impose more prior knowledge on the signal, whereas $\lambda \to 0$ prioritizes a low data-fidelity cost.

Usual choices for regularization norm are Tikhonov L_2 norm $\mathcal{R}(f) = ||\mathrm{L}f||_{L_2}^2$ and gTV (generalized total-variation) $\mathcal{R}(f) = ||\mathrm{L}f||_{\mathcal{M}}$. The latter is the continuous counterpart of the discrete ℓ_1 norm, known for its sparsity promoting property. The theory of compressed sensing (CS) investigates discrete inverse problems with ℓ_1 norm [1], [2], as well as continous inverse problems - infinite dimensional CS [3], [4].

In this paper, we employ gTV as our regularization norm to enforce the sparsity of the reconstructed signal.

B. Self-similarity and fractional derivatives

Self-similar stochastic processes [5], [6] and their most prominent representatives - fractional Brownian motions (fBm), are known to be useful in modeling and analyzing many real-world signals. Their applications to signal processing [7], [8], image processing [9], [10], biomedical signal analysis [11], [12], turbulence analysis [13], [14], etc. have been investigated extensively. There have also been research efforts in applying wavelet analysis to such stochastic processes [15], [16], as well as to investigate their connection with splines and fractional derivatives [17], [18].

Self-similar stochastic processes can be obtained as solutions s of stochastic differential equations of the form

$$\mathrm{L}s = w, \tag{2}$$

where L is a scale-invariant LSI operator, and w is a self-similar innovation [19]. As a special case, applying operator L to fBm yields Gaussian white noise. Furthermore, the scale-invariance conditions limit the choice of operator L and innovation w. In the case of 1-D processes, the class of scale-invariant LSI operators consists of generalized fractional derivatives (Proposition 2 [17]), whereas the class of self-similar innovations consists of α-stable processes [19].

*School of Electrical Engineering, University of Belgrade, 11000 Belgrade, Serbia (email: sstojanovic97@hotmail.com)

†Biomedical Imaging Group, Ecole Polytechnique Federale de Lausanne, 1015 Lausanne, Switzerland (email: thomas.debarre@epfl.ch; michael.unser@epfl.ch)

C. Inverse problems for reconstructing self-similar processes

Applying fractional derivative to self-similar process s yields innovation w, implying that the fractional derivatives are whitening operators for self-similar processes. We make use of this property and employ fractional derivatives as our regularization operator L. Moreover, there are recent studies of fractional derivatives as regularization operators for reconstructing Gaussian bridges [20].

It is known that the solution of inverse problem (1) with Tikhonov regularization [21] is the minimum mean-square error (MMSE) solution only for stationary processes. The same result was obtained in the periodic setting, with empirical evidence that variational and MMSE solutions are practically indistinguishable under certain conditions (see Section V in [20]).

It has been shown that processes s stemming from α-stable innovations w with $0 < \alpha < 2$ are inherently sparse [22], which is not the case for Gaussian white noise ($\alpha = 2$). Therefore, using the sparsity-promoting $||\cdot||_{\mathcal{M}}$ norm to reconstruct SαS processes is a natural choice. We thus propose to use a regularization term $\mathcal{R}(f) = ||\mathrm{L}\{f\}||_{\mathcal{M}}$ for reconstructing self-similar processes, and validate this choice experimentally.

D. Periodic Setting

For practical purposes, we adopt a periodic setting. This approach is valid not only for periodic signals, but also for signals with bounded support which can be periodized. A key benefit of the periodic setting is the availability of the Fourier series expansion, which conveys many advantages, most notably - computational simplicity. Therefore, given some fractional operator L, we want to reconstruct a continuous periodic function f using an inverse problem of the form:

$$\min_{f} \ ||\boldsymbol{\nu}(f) - \boldsymbol{y}||_2^2 + \lambda ||\mathrm{L}\{f\}||_{\mathcal{M}} \ . \tag{3}$$

In a non-periodic setting, it was shown that this type of inverse problems has nonuniform L-splines as solutions [23], [24]. These results were later extended to the periodic setting in [25], in which it is proved that solution of problem (3) is a nonuniform periodic L-spline.

E. Discretization

Discretization based on the measure theory aims to recover the exact locations of Dirac impulses [26]–[31]. Also, there are grid-based approaches which aim to recover signals on a grid [32], [33]. Following these works, we adopt a grid-based approach in our framework. We use a periodic B-spline basis [34], [35] and show that it spans the space of uniform periodic L-splines. This choice of basis is guided by the representer theorem in [25] which states that (3) has periodic spline solutions. This choice of basis leads to the following discrete optimization problem:

$$\min_{\mathbf{c} \in \mathbb{R}^N} ||\mathbf{H}\mathbf{c} - \mathbf{y}||_2^2 + \lambda ||\mathbf{L}\mathbf{c}||_1 \ , \tag{4}$$

where $\mathbf{H} \in \mathbb{R}^{M \times N}$ is the system matrix, $\mathbf{L}$ is the finite difference-like regularization matrix, and $\mathbf{c} \in \mathbb{R}^N$ is a vector of coefficients of the B-spline basis representation. Moreover, the approximation error induced by discretization can be made arbitrarily small by reducing the grid step size.

F. Outline

The present paper is organized as follows. In Section II, we set the stage by presenting our periodic setting and our inverse problem, along with a representer theorem for periodic signals, introduced in [20]. We also familiarize the reader with the notion of periodic splines. Then, in Section III, we introduce fractional derivatives and their periodic versions. In Section IV, we turn our attention to self-similar processes. We describe how to generate them, their properties, and their connections with fractional derivatives. In Section V, we define fractional B-splines, their periodic counterparts and show that they span the space of uniform periodic L-splines which we use as search space in our discretization. In Section VI, we formulate the discretized inverse problem and show that it amounts to a standard ℓ_1-regularized problem. We also introduce the multiresolution strategy of our algorithm. Then, in Section VII, we present our experimental setting. We conclude with the experimental results which show that our framework results in efficient sparse signal reconstruction for both deterministic and stochastic signals.

II. Periodic Setting

Here will be given a short review of the representer theorem for periodic signals and related concepts introduced in [20], [25].

A. Periodic Signals

In order to simplify notations, without loss of generality, we will only consider periodic signals with period $T = 1$.

We define the interval of interest as $\mathbb{T} = [0, 1)$. Let $\mathcal{S}(\mathbb{T})$ be the space of 1-periodic functions $f : \mathbb{T} \to \mathbb{R}$ that are infinitely differentiable. The topological dual of $\mathcal{S}(\mathbb{T})$ is $\mathcal{S}'(\mathbb{T})$, the space of 1-periodic generalized functions.

Let Ш be a 1-periodic Dirac comb defined by:

$$\text{Ш} = \sum_{k \in \mathbb{Z}} \delta(\cdot - k) \tag{5}$$

where $\delta(\cdot)$ is a Dirac impulse. Using the Dirac comb, any suitable function f can be periodized as follows:

$$f_{per}(x) = \sum_{k \in \mathbb{Z}} f(x - k) = (f * \text{Ш})(x) \tag{6}$$

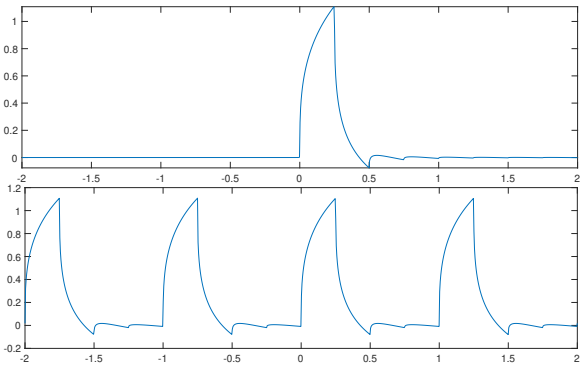

Figure 1: Classical and periodic ($T = 1$) non-centered fractional B-spline of order 1.3 with grid step $h = \frac{1}{4}$

The theory of Fourier series states that any periodic generalized function $g \in \mathcal{S}'(\mathbb{T})$ can be uniquely decomposed as:

$$g = \sum_{k\in\mathbb{Z}} \widehat{g}[k] e_k, \tag{7}$$

where e_k is a complex sinusoid $e_k : x \mapsto e^{j2\pi xk}$. Therefore, g is characterized by its Fourier series coefficients $(\widehat{g}[k])_{k\in\mathbb{Z}}$ defined by:

$$\widehat{g}[k] = \int_{-1/2}^{1/2} g(x) e^{-j2\pi kx} dx \tag{8}$$

The duality product of $f \in \mathcal{S}(\mathbb{T})$ and $g \in \mathcal{S}'(\mathbb{T})$ is given by:

$$\langle f, g\rangle = \sum_{k\in\mathbb{Z}} \widehat{f}[k]\widehat{g}[k]^* \tag{9}$$

(Parseval's theorem), where $\widehat{g}[k]^*$ is the complex conjugate of $\widehat{g}[k]$.

B. Periodic LSI operators and splines

It is well known that for any continuous, linear and shift-invariant (LSI) operator $\mathrm{L} : \mathcal{S}'(\mathbb{T}) \to \mathcal{S}'(\mathbb{T})$ and for any $f \in \mathcal{S}'(\mathbb{T})$, we have:

$$\mathrm{L}\{f\} = \sum_{k\in\mathbb{Z}} \widehat{L}[k]\widehat{f}[k] e_k \tag{10}$$

where $(\widehat{L}[k])_{k\in\mathbb{Z}}$ is the Fourier series of $\mathrm{L}\{\text{Ш}\}$. In other words, any continous LSI operator L has complex sinusoids e_k as eigenfunctions, and the $(\widehat{L}[k])_{k\in\mathbb{Z}}$ as eigenvalues.
We define the null-space of the operator L as follows:

$$\mathcal{N}_{\mathrm{L}} = \{f \in \mathcal{S}'(\mathbb{T}) : \mathrm{L}\{f\} = 0\}. \tag{11}$$

In the case of continuous LSI operators, the null space can be expressed as:

$$\mathcal{N}_{\mathrm{L}} = \mathrm{Span}\{e_k : \widehat{L}[k] = 0\}. \tag{12}$$

We focus on the following class of LSI operators:

Definition 1. *(Spline-admissible operator): Let* $\mathrm{L} : \mathcal{S}'(\mathbb{T}) \to \mathcal{S}'(\mathbb{T})$ *be a continuous LSI operator. We say that* L *is spline-admissible if it has a finite null space (*$\dim \mathcal{N}_{\mathrm{L}} < \infty$*) and the sequence* $\left(\frac{1}{\widehat{\mathrm{L}}[k]}\right)_{k\in\mathbb{Z}}$ *is slowly growing.*

The first requirement - the finite null space - is satisfied for most commonly-used operators, e.g. differential operators and fractional derivatives [25]. Finally, we now define periodic L-splines.

Definition 2. *(Periodic* L*-spline): Let* L *be a spline admissible operator. Then, a function* $f \in \mathcal{S}'(\mathbb{T})$ *is a periodic* L*-spline if:*

$$\mathrm{L}\{f\}(x) = \sum_{k=1}^{K} a_k \text{Ш}(x - x_k), \tag{13}$$

where $a_k \in \mathbb{R}$, $x_k \in \mathbb{T}$ *and* $K \in \mathbb{N}$.

We now detail the construction of the native space of our operator L. First, let $\mathcal{C}_0(\mathbb{T})$ be the space of continous 1-periodic functions. Let $\mathcal{M}(\mathbb{T}) \subset \mathcal{S}'(\mathbb{T})$ be the space of periodic finite Radon measures, defined as the continuous dual of $\mathcal{C}_0(\mathbb{T})$. Then, $\mathcal{M}(\mathbb{T})$ is a Banach space equipped with dual norm $||\cdot||_{\mathcal{M}}$ defined by:

$$||w||_{\mathcal{M}} = \sup_{\phi\in\mathcal{S}(\mathbb{T}):||\phi||_\infty=1} \langle w, \phi\rangle \tag{14}$$

for any $w \in \mathcal{M}(\mathbb{T})$. The norm $||\cdot||_{\mathcal{M}}$ associated with the space $\mathcal{M}(\mathbb{T})$ is a generalization of the L_1 norm. More precisely, we have $L_1(\mathbb{T}) \subset \mathcal{M}(\mathbb{T})$ and $||f||_{L_1} = ||f||_{\mathcal{M}}$ for any $f \in L_1(\mathbb{T})$. Also, the space $\mathcal{M}(\mathbb{T})$ includes the Dirac comb for which $||\text{Ш}(\cdot - x_0)||_{\mathcal{M}} = 1$, for any $x_0 \in \mathbb{T}$. The native space $\mathcal{M}_{\mathrm{L}}(\mathbb{T})$ of an admissible operator L is:

$$\mathcal{M}_{\mathrm{L}}(\mathbb{T}) = \Big\{f \in \mathcal{S}'(\mathbb{T}) : \mathrm{L}\{f\} \in \mathcal{M}(\mathbb{T})\Big\}. \tag{15}$$

This native space is the largest space for which $||\mathrm{L}\{f\}||_{\mathcal{M}}$ is well-defined. It can be shown that the predual of $\mathcal{M}_{\mathrm{L}}(\mathbb{T})$ can be expressed as the direct sum:

$$\mathcal{C}_{\mathrm{L}}(\mathbb{T}) = \mathrm{L}^*(\mathcal{C}_0(\mathbb{T})) \oplus \mathcal{N}_{\mathrm{L}} \tag{16}$$

where L^* is the adjoint of L.

C. Representer Theorem

We now present the representer theorem for periodic signals introduced in [25].

Theorem 1. *(Representer theorem): Let* L *be a spline-admissible operator with null space* $\mathcal{N}_{\mathrm{L}}$*. Let* $\boldsymbol{\nu} = (\nu_1, ..., \nu_M)$*, where* $\nu_m \in \mathcal{C}_{\mathrm{L}}(\mathbb{T})$ *for* $m = 1, \ldots, M$*, be the continuous forward model such that* $\boldsymbol{\nu}(p) = 0$ *if and only if* $p = 0$*. Then, the solution set of the problem:*

$$\mathcal{S} = \underset{f\in\mathcal{M}_{\mathrm{L}}(\mathbb{T})}{\arg\min} ||\boldsymbol{\nu}(f) - \boldsymbol{y}||_2^2 + \lambda||\mathrm{L}\{f\}||_{\mathcal{M}} \tag{17}$$

is a non-empty, convex, weak-compact set. Moreover, the extreme points of* $\mathcal{S}$ *are periodic splines satisfying:*

$$\mathrm{L}\{f\} = \sum_{k=1}^{K} a_k \text{Ш}(\cdot - x_k), \tag{18}$$

where the coefficients $a_k \in \mathbb{R}$, $x_k \in \mathbb{T}$ *for* $k = 1, \ldots, K$, *and the sparsity* K *is bounded by* $K \leq M$.

The representer theorem is powerful in at least two ways. It states that any extreme point of the solution set is a periodic L-spline, which motivates our use of periodic splines as basis functions to discretize problem (16). Moreover, as a result of the sparsity-promoting effect of the $||\cdot||_{\mathcal{M}}$ norm, the number of knots K is bounded by the number of measurements M.

III. The (γ, τ)-Fractional Derivatives

Common choices for the regularization operator L are the first and second order derivative - $\mathrm{L} = \mathrm{D}$ (leading to TV regularization), and $\mathrm{L} = \mathrm{D}^2$. In the following section, we introduce a broader class known as fractional derivatives, that were studied extensively in [18], [36].

Let L be a fractional operator whose Fourier transform is defined by:

$$\widehat{L}_\tau^\gamma(w) = (j\omega)^{\frac{\gamma}{2}+\tau}(-j\omega)^{\frac{\gamma}{2}-\tau} \tag{19}$$

where $\gamma > 0$ and τ are real parameters. When $\tau = \frac{\gamma}{2}$ and $\gamma \in \mathbb{N}$, we recover the γ-th order derivative.

A. Periodic (γ, τ)-Fractional Derivatives

We now introduce fractional derivatives in the periodic setting. From (10), we see that any spline-admissible operator L is uniquely determined by its Fourier series. Using (19), we can express the Fourier series of the periodic (γ, τ)-operator $(\widehat{L}[k])_{k\in\mathbb{Z}}$ as:

$$\widehat{L}[k] = (j2\pi k)^{\frac{\gamma}{2}+\tau}(-j2\pi k)^{\frac{\gamma}{2}-\tau} \tag{20}$$

for every $k \in \mathbb{Z}$. Note that the underlying operator $\mathrm{L} : f \in \mathcal{S}'(\mathbb{T}) \mapsto \sum_{k\in\mathbb{Z}} \widehat{f}[k]\widehat{L}[k]e_k$ coincides with (19) over $\mathcal{S}'(\mathbb{T})$.

Equation (20) implies that $\widehat{L}[k] = 0$ if and only if $k = 0$. We conclude that $\mathcal{N}_{\mathrm{L}} = \mathrm{span}\{1\}$, which conforms with Definition 1.

Also note that, since $\widehat{L}[0] = 0$, there are implicit additional constraints on the coefficients a_k from the periodic spline definition (13). Namely, these coefficients must satisfy $\sum_{k=0}^{N-1} a_k = 0$.

IV. Self-Similar Processes

We now introduce stochastic processes that are inherently connected with fractional derivatives. Indeed, fractional operators are the only 1D scale-invariant operators. It has been shown that the MMSE estimator for a statistically self-similar stochastic process is a fractional spline [17]. The foundation of the following subsections is the theory of sparse stochastic processes [19].

We say that a real-valued stochastic process s is self-similar if for any scale parameter $a > 0$, we have:

$$s(\cdot) \overset{\Delta}{=} a^H s\left(\frac{\cdot}{a}\right) \tag{21}$$

where $H > 0$ is the Hurst exponent, and by $\overset{\Delta}{=}$ we denote the equivalence in law.

Self-similar processes can be specified as solutions $s \in \mathcal{S}'(\mathbb{T})$ of fractional stochastic differential equations (SDEs) of the following form:

$$\mathrm{L}_s s = w, \tag{22}$$

where w is the innovation, and L_s is the fractional derivative operator of order γ_s and phase parameter τ_s. Notice that the process s depends on the innovation w, as well as the parameters γ_s and τ_s. The expression (22) can be regarded as a whitening of the process s [17]. As stated earlier, fractional derivatives form the complete family of 1-D scale-invariant LSI operators of a given order. Therefore, they specify the broadest class of 1-D self-similar processes that are solutions of fractional SDEs.

A. Symmetric-α-Stable Processes

Given some scale-invariant operator L_s, in order for the process s to be a self-similar process, the innovation w in (22) must be self-similar as well. This implies that innovation w has to be an α-stable noise (see Section 7.5 in [19]).

The characteristic function of Symmetric-α-Stable (SαS) processes is given by:

$$\widehat{p}(\omega; \alpha, s_0) = e^{-|s_0\omega|^\alpha} \tag{23}$$

where $\alpha \in (0, 2]$ is the degree, and $s_0 \in \mathbb{R}^+$ is the scale parameter. In the following discussion, we will only consider the case $s_0 = 1$. In the special case of $\alpha = 1$, we recover the Cauchy distribution, and for $\alpha = 2$, the Gaussian distribution.

It can be shown that a solution s of the SDE (22) with innovation $w = w_\alpha$, where w_α is a SαS noise with parameter α, is a self-similar generalized stochastic process s [19]. These random processes s are called fractional stable motions (fSm); they generalize fractional Brownian motion that corresponds to the Gaussian case.

The parameter α can be seen as a measure of sparsity (i.e. compressibility) of s [22]. Stable self-similar processes that result from fractional integration of a SαS-process are inherently sparse for $\alpha < 2$. Smaller values of α correspond to sparser processes, whereas the upper limit $\alpha = 2$ correspond to Gaussian processes, that are not sparse.

As already mentioned, the solution of inverse problem (1) with Tikhonov L_2 regularization is the minimum mean-square error (MMSE) solution only for stationary processes [20], [21]. Despite this theoretical suboptimality, variational and MMSE solutions are practically indistinguishable [20]. In Section VIII, we investigate the effect of replacing fBm processes by their generalization (fSm) with

gTV and L_2 regularization on the performance of fractional splines as estimators. Since gTV is inherently connected with reconstruction of sparse signals, we expect to efficiently reconstruct sparse SαS-processes using gTV.

V. The (γ, τ)-Fractional Splines

From the practical point of view, differential operators can sometimes be replaced by their discrete counterparts - finite differences. The Fourier transform of the generalized finite-difference operator is given by:

$$\widehat{\Delta}_\tau^\gamma(\omega) = (1 - e^{-j\omega})^{\frac{\gamma}{2}+\tau}(1 - e^{j\omega})^{\frac{\gamma}{2}-\tau} . \quad (24)$$

It follows from the Taylor's expansion $e^{j\omega} = 1 + j\omega + \mathcal{O}(\omega^2)$ that the finite difference operator is a discrete approximation of the derivative. In fact, the connection between these two operators is given by fractional B-splines.

A. Fractional B-splines

The expression for generalized (γ, τ)-fractional B-splines in the Fourier domain is given by:

$$\begin{aligned}\widehat{\beta}_\tau^\gamma(\omega) &= \frac{\widehat{\Delta}_\tau^\gamma(\omega)}{\widehat{L}_\tau^\gamma(w)} \quad (25)\\ &= \left(\frac{1 - e^{-j\omega}}{j\omega}\right)^{\frac{\gamma}{2}+\tau}\left(\frac{1 - e^{j\omega}}{-j\omega}\right)^{\frac{\gamma}{2}-\tau}\end{aligned}$$

We will now give a short overview of the properties of fractional B-splines (for more information, we refer to [36], [37]):

- lack of positivity and compact support when $\gamma \notin \mathbb{N}$
- the decay of fractional B-splines is $\beta_\tau^\gamma(x) \propto |x|^{-\gamma-1}$ when $|x| \to \infty$
- ability to reproduce polynomials of degree $\lceil \alpha \rceil$
- fractional order of approximation γ, meaning that $||f - \mathcal{P}_h f||_{L^2}$ decays like h^γ when $h \to 0$, where $\mathcal{P}_h$ is an orthogonal projection operator onto the space of uniform fractional B-splines at scale h
- satisfies the two-scale relation
- L_τ^γ-splines are scale-invariant of order γ, meaning that $\mathrm{L}\{s(t/T)\} = \sum_{k\in\mathbb{Z}} T^{1-\gamma} a[k]\delta(t - kT)$ with $a \in \ell_\infty(\mathbb{Z})$ for any scale $T > 0$, where $s(t)$ is a L_τ^γ-spline

The family of generalized (γ, τ)-fractional B-splines is the most general family of fractional splines.
In the case when $\tau = \frac{\gamma}{2}$, we get the causal fractional B-splines:

$$\widehat{\beta}_{\frac{\gamma}{2}}^\gamma(\omega) = \left(\frac{1 - e^{-j\omega}}{j\omega}\right)^\gamma . \quad (26)$$

Another noteworthy case is $\tau = 0$, which leads to symmetric fractional B-splines:

$$\widehat{\beta}_0^\gamma(\omega) = \left(\frac{1 - e^{-j\omega}}{j\omega}\right)^{\frac{\gamma}{2}}\left(\frac{1 - e^{j\omega}}{-j\omega}\right)^{\frac{\gamma}{2}} . \quad (27)$$

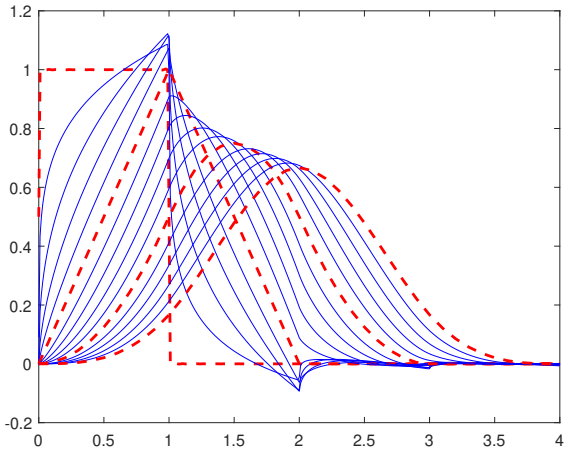

Figure 2: Causal fractional B-splines of order 1 to 4 with step 0.2 *(red dashed lines - integer γ, blue solid lines - non-integer γ)*

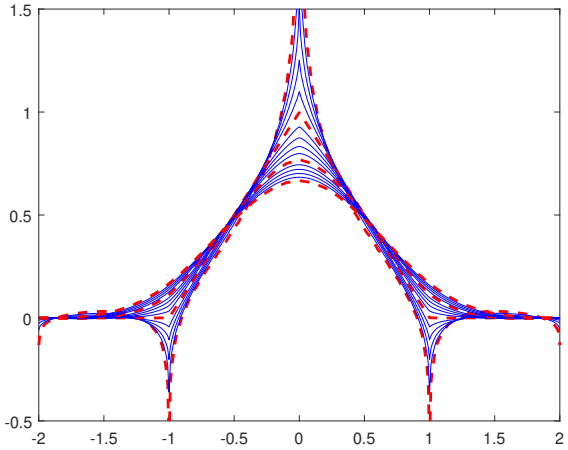

Figure 3: Centered/symmetric fractional B-splines of order 1 to 4 with step 0.2 *(red dashed lines - integer γ, blue solid lines - non-integer γ)*

In Figures 2 and 3, we plot causal and symmetric fractional B-splines, respectively, for different values of γ.
In all that follows, for simplicity of notation, we drop the γ, τ and use the notation β instead of β_τ^γ.

B. Scaled B-splines

The fractional (γ, τ) B-splines with knot spacing $h > 0$ are defined by $\beta_h(x) = \beta(\frac{x}{h})$ which yields:

$$\begin{aligned}\widehat{\beta}_h(\omega) &= h\widehat{\beta}(h\omega) = \quad (28)\\ &= \frac{1}{h^{\gamma-1}}\left(\frac{1 - e^{-jh\omega}}{j\omega}\right)^{\frac{\gamma}{2}+\tau}\left(\frac{1 - e^{jh\omega}}{-j\omega}\right)^{\frac{\gamma}{2}-\tau}\end{aligned}$$

From the Fourier-domain representation of scaled fractional B-splines (28) and the differential operator (19), we have:

$$\mathrm{L}\{\beta_h\} = \frac{1}{h^{\gamma-1}}\sum_{k\in\mathbb{Z}} d[k]\delta(\cdot - kh) \quad (29)$$

where d is defined by its z-transform:

$$\Delta(z) = (1 - z^{-1})^{\frac{\gamma}{2}+\tau}(1 - z)^{\frac{\gamma}{2}-\tau}. \quad (30)$$

Note that d has finite support $\text{supp}(d) = \{-\frac{\gamma}{2} + \tau, \ldots, \frac{\gamma}{2} + \tau\}$ when:

$$-\frac{\gamma}{2} + \tau,\ \frac{\gamma}{2} + \tau \in \mathbb{Z} \tag{31}$$

The size of $\text{supp}(d)$ is then equal to $\gamma + 1$ and is thus independent of τ.

C. Periodic B-splines

Let us now define periodic B-splines as:

$$\beta_{per,h}(x) = \sum_{k\in\mathbb{Z}} \beta_h(x-k) = (\beta_h * \text{Ш})(x) \tag{32}$$

where $\beta_h(\cdot)$ is the scaled B-spline defined in (28). Notice that we used (6) to represent the periodic signal as a convolution. As previously stated, the decay of fractional B-splines is $\beta(x) \propto |x|^{-\gamma-1}$ when $|x| \to \infty$. Therefore, for $\gamma > 0$ the sum above is convergent and $\beta_{per}(x)$ is well defined.
Since $\beta_{per,h}$ is 1-periodic, it has a Fourier series expansion of the form:

$$\beta_{per,h}(x) = \sum_{k\in\mathbb{Z}} \widehat{\beta}_{per,h}[k] e^{j2\pi kx} \tag{33}$$

where $\widehat{\beta}_{per,h}[k]$ are the Fourier series coefficients that can be easily computed using standard Fourier analysis:

$$\widehat{\beta}_{per,h}[k] = \widehat{\beta}_h(2\pi k) = \frac{1}{h^{\gamma-1}} \left(\frac{1-e^{-jh2\pi k}}{j2\pi k}\right)^{\frac{\gamma}{2}+\tau} \times \left(\frac{1-e^{jh2\pi k}}{-j2\pi k}\right)^{\frac{\gamma}{2}-\tau} \tag{34}$$

for all $k \in \mathbb{Z}$.
We then define the periodized filter $d_{per}[k] = \sum_{m\in\mathbb{Z}} d[k - Nm]$, for all $k \in \mathbb{Z}$, where $N = \frac{1}{h}$ and $d[k]$ is defined in (30). Note that d_{per} is equal to d on one period if the finite-support condition (31) is satisfied. Since d_{per} is the periodization of d, then from (30) we have:

$$\Delta_{per}[k] = \Delta(2\pi k) = \left(1-e^{-jh2\pi k}\right)^{\frac{\gamma}{2}+\tau} \times \left(1-e^{jh2\pi k}\right)^{\frac{\gamma}{2}-\tau} \tag{35}$$

for $k \in \mathbb{Z}$. To obtain the expression for $d_{per}[k]$ we use the inverse discrete Fourier transform (DFT):

$$d_{per}[k] = \frac{1}{N} \sum_{n=0}^{N-1} \Delta_{per}[n] e^{j2\pi kn/N}. \tag{36}$$

Note that in the following sections, $C[k]$ can denote both the DFT of a vector $\mathbf{c} \in \mathbb{R}^N$ as well as the discrete time Fourier transform (DTFT) of an N-periodic sequence $(c[n])_{n\in\mathbb{Z}}$.
We now define a search space that is a discretized version of the native space $\mathcal{M}_{\text{L}}(\mathbb{T})$ defined by (15). We denote it by $\mathcal{M}_{\text{L},h}(\mathbb{T})$ and define it as the space of periodic splines with knots on the uniform grid of size h:

$$\mathcal{M}_{\text{L},h}(\mathbb{T}) = \left\{ f \in \mathcal{S}'(\mathbb{T}) : \text{L}\{f\} = \sum_{k=0}^{N-1} a_k \text{Ш}(\cdot - kh) \right\} \tag{37}$$

where $N = \frac{1}{h}$ and $a_k \in \mathbb{R}$ such that $\sum_{k=0}^{N-1} a_k = 0$. An important property of this space is that it is spanned by periodic B-splines, as we show in the following proposition.

Proposition 1. *The space $\mathcal{M}_{\text{L},h}(\mathbb{T})$ can be equivalently expressed as:*

$$\mathcal{M}_{\text{L},h}(\mathbb{T}) = \left\{ f = \sum_{k=0}^{N-1} c_k \beta_{per,h}(\cdot - kh) : \mathbf{c} \in \mathbb{R}^N \right\} \tag{38}$$

The proof is given in Appendix A.
Another interesting property is given in the following proposition.

Proposition 2. *For any grid size $h = 1/2^k$, with $k > 0$, the following holds:*

$$\mathcal{M}_{\text{L},h}(\mathbb{T}) \subset \mathcal{M}_{\text{L},h/2}(\mathbb{T}) \tag{39}$$

Moreover, any $f = \sum_{k=0}^{N-1} c_{h,k} \beta_{per,h}(\cdot - kh) \in \mathcal{M}_{\text{L},h}(\mathbb{T})$ can be represented as $f = \sum_{k=0}^{2N-1} c_{h/2,k} \beta_{per,h/2}(\cdot - kh/2) \in \mathcal{M}_{\text{L},h/2}(\mathbb{T})$ with coefficients $c_{h/2,k}$ defined by:

$$C_{h/2}[k] = C_h[k] 2^{-\gamma+1} (1 + e^{-jh\pi k/N})^{\frac{\gamma}{2}+\tau} \times (1 + e^{jh\pi k/N})^{\frac{\gamma}{2}-\tau} \tag{40}$$

where $(C_h[k])_{k\in\mathbb{Z}}$ is the DFT of $\mathbf{c}_h$.

Proof. We prove that any $f \in \mathcal{M}_{\text{L},h}(\mathbb{T})$ is also an element of $\mathcal{M}_{\text{L},h/2}(\mathbb{T})$. Let $c_{h,k}$ be the B-spline coefficients of $f \in \mathcal{M}_{\text{L},h}(\mathbb{T})$. Then, we have:

$$\begin{aligned} f(x) &= \sum_{k=0}^{N-1} c_{h,k} \beta_{per,h}(x - kh) \\ &= \sum_{k=0}^{N-1} c_{h,k} \sum_{m\in\mathbb{Z}} \widehat{\beta}_{per,h}[m] e^{j2\pi m(x-kh)} \\ &= \sum_{m\in\mathbb{Z}} \widehat{\beta}_{per,h}[m] e^{j2\pi mx} \sum_{k=0}^{N-1} c_{h,k} e^{-j2\pi mk/N} \\ &= \sum_{m\in\mathbb{Z}} \widehat{\beta}_{per,h}[m] C_h[m] e^{j2\pi mx} \end{aligned} \tag{41}$$

From (34) we obtain the two-scale relation:

$$\widehat{\beta}_{per,h}[k] = 2^{1-\gamma} (1 + e^{-jh\pi k})^{\frac{\gamma}{2}+\tau} \times (1 + e^{jh\pi k})^{\frac{\gamma}{2}-\tau} \widehat{\beta}_{per,h/2}[k]. \tag{42}$$

and using this relation we choose coefficients $C_{h/2}[k]$ as in (40). This choice implies that $\widehat{\beta}_{per,h}[k] C_h[k] = \widehat{\beta}_{per,h/2}[k] C_{h/2}[k]$, for any $k \in \mathbb{Z}$. Since the Fourier series decomposition is unique, we thus have $f(x) = \sum_{k=0}^{2N-1} c_{h/2,k} \beta_{per,h}(x - kh/2)$, where $\mathbf{c}_{h/2}$ is the inverse DFT of $C_{h/2}$. We conclude that $f \in \mathcal{M}_{\text{L},h/2}(\mathbb{T})$. □

VI. Discretization

The representer theorem (Theorem 1) does not specify the knot locations $x_k \in \mathbb{T}$. In order to discretize Problem (17), we force the knots x_k to be on a grid of adjustable size $h > 0$, and let $N = \frac{1}{h}$ be the number of grid points in one period. Then, we represent the reconstructed signal $f \in \mathcal{M}_{\mathrm{L},h}(\mathbb{T})$ in the periodic B-splines basis (38) as:

$$f(x) = \sum_{k=0}^{N-1} c_k \beta_{per,h}(x - kh) \tag{43}$$

where $\mathbf{c} = (c_0, ..., c_{N-1}) \in \mathbb{R}^N$. In this way, we are restricting the search space to $\mathcal{M}_{\mathrm{L},h}(\mathbb{T})$, defined in (37).

Although this restriction results in an approximation error, it can be made arbitrarily small by reducing the grid size. Therefore, choosing $\mathcal{M}_{\mathrm{L},h}(\mathbb{T})$ as our search space, we discretize our inverse problem in an exact way. Furthermore, the discretized problem is a standard convex discrete problem, and can be solved using off-shelf algorithms.

A. Regularization Term

We now recall the equation (58) from Appendix A, that is obtained by applying the differential operator L to a signal of the form (38):

$$\mathrm{L}\{f\}(x) = \frac{1}{h^{\gamma-1}} \sum_{k=0}^{N-1} (\mathbf{c} * d_{per})_k \text{Ш}(x - kh)$$

Now, we can express $||\mathrm{L}\{f\}||_{\mathcal{M}}$ using the ℓ_1-norm:

$$||\mathrm{L}\{f\}||_{\mathcal{M}} = \frac{1}{h^{\gamma-1}} ||\mathbf{c} * d_{per}||_1 \tag{44}$$

Our initial regularization term which was defined using the continuous operator L and the continuous function f can thus be expressed as the ℓ_1 norm of the cyclic convolution of discrete signals. We then define the regularization matrix $\mathbf{L} \in \mathbb{R}^{N \times N}$ as:

$$\mathbf{Lc} = \frac{1}{h^{\alpha}} \mathbf{c} * d_{per} \tag{45}$$

B. Discrete Forward Model

Applying the forward model $\boldsymbol{\nu}$ to signal f of the form (38) and using the linearity of the forward model, we get:

$$\begin{aligned} \boldsymbol{\nu}(f) &= \boldsymbol{\nu}\left(\sum_{k=0}^{N-1} c_k \beta_{per,h}(\cdot - kh) \right) \\ &= \sum_{k=0}^{N-1} c_k \boldsymbol{\nu}(\beta_{per,h}(\cdot - kh)) = \sum_{k=0}^{N-1} c_k \mathbf{h}_k \end{aligned} \tag{46}$$

where $\mathbf{h}_k = \boldsymbol{\nu}(\beta_{per,h}(\cdot - kh))$. Therefore, the discretization of the continuous forward model $\boldsymbol{\nu}$ is the system matrix $\mathbf{H} \in \mathbb{R}^{M \times N}$ defined by:

$$\mathbf{H} = (\mathbf{h}_0, \ldots, \mathbf{h}_{N-1}) : \quad \mathbf{h}_k = \boldsymbol{\nu}(\beta_{per,h}(\cdot - kh)). \tag{47}$$

C. Discretized Problem

By combining the previous subsections, we get the discretized version of problem (17):

$$\mathcal{S}_{\text{finite}} = \underset{\mathbf{c} \in \mathbb{R}^N}{\arg\min} ||\mathbf{Hc} - \mathbf{y}||_2^2 + \lambda ||\mathbf{Lc}||_1, \tag{48}$$

where $\mathbf{L} \in \mathbb{R}^{N \times N}$ is the regularization matrix defined in (45) and $\mathbf{H} \in \mathbb{R}^{M \times N}$ is the system matrix defined in (47).

Discrete optimization problems of the form (48) can be solved using standard solvers such as ADMM [38]. However, there is no guarantee that the obtained solution $\mathbf{c}^*$ will be a desired sparse solution in the sense that $||\mathbf{Lc}^*||_0 \leq M$. We therefore adapt a two-step algorithm introduced in [32]:

- using ADMM, we solve the finite discretized optimization problem (48) and obtain a solution $\mathbf{c}_{\text{ADMM}} \in \mathcal{S}_{\text{finite}}$. Then, we compute $\mathbf{y}_\lambda$ as $\mathbf{y}_\lambda = \mathbf{Hc}_{\text{ADMM}}$, which does not depend which solution $\mathbf{c}_{\text{ADMM}}$ is reached.
- using $\mathbf{y}_\lambda$, we can solve the following constrained optimization problem:

$$\underset{\mathbf{c} \in \mathbb{R}^N}{\arg\min} ||\mathbf{Lc}||_1 \quad \textit{s.t.} \quad \mathbf{Hc} = \mathbf{y}_\lambda, \tag{49}$$

that has the same solution set $\mathcal{S}_{\text{finite}}$. This problem can be recast as a linear program, and solved by applying the simplex algorithm [39], which is known to converge to an extreme point of the solution set $\mathcal{S}_h^{\text{LP}}$.

The discrete representer theorem (Theorem 2 in [33]) states that problem (48) has some solutions that are sparse. Namely, $\mathcal{S}_{\text{finite}}$ is a compact convex set whose extreme points $\mathbf{c}^*$ satisfy $||\mathbf{Lc}^*||_0 \leq M$, where $||\cdot||_0$ is the ℓ_0 "norm". Therefore, by applying this algorithm we reach a sparse extreme point $\mathbf{c}^* \in \mathcal{S}_{\text{finite}}$.

D. Multiresolution Strategy

The optimal choice of the grid size h is data-dependent. Therefore, following the multiresolution strategy presented in [33], we recursively split the grid in half and repeat the algorithm presented in previous section for the finer grid.

We use (40) to compute the starting coefficients $\mathbf{c}_{h/2}$ of the following iteration based on the coefficients $\mathbf{c}_h$ of the previous one. In this way, we have a warm-start initialization that reduces the computation time of our multiresolution algorithm.

This algorithm allows us to decrease the grid size until the desired level of accuracy is achieved. Given some tolerance parameter $\epsilon > 0$, the stopping criterion is reached once the relative decrease of cost of two consequent iterations is smaller than ϵ.

VII. Experimental Setting

A. Measurements

In order to account for the noise in our acquisition system, we model measurements in the following form:

$$\mathbf{y} = \boldsymbol{\nu}(f_0) + n$$

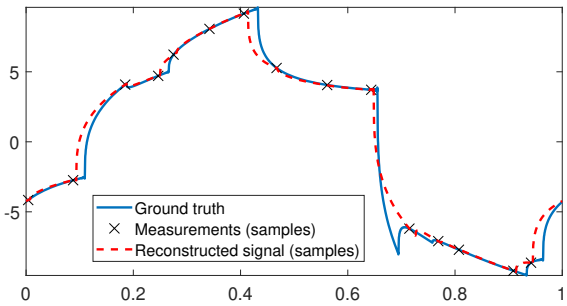

Figure 4: (γ, τ)-fractional periodic non-centered B-spline with $\gamma = 1.3$, $\tau = \frac{\gamma}{2}$. Sparsity: 27 after ADMM, 15 after Simplex. SNR = 17.10 dB.

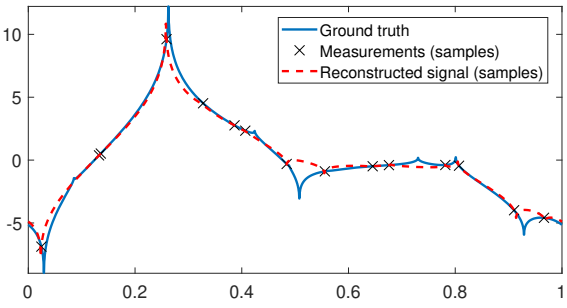

Figure 5: (γ, τ)-fractional periodic centered B-spline with $\gamma = 1.3$, $\tau = 0$. Sparsity: 13 after ADMM, 13 after Simplex. SNR = 16.04 dB.

where n is the Gaussian white noise. Also, we consider two cases of forward model $\boldsymbol{\nu}$ - ideal sampling and Fourier sampling.

1) Ideal sampling: In the case of ideal sampling, the measurement operator is:

$$\boldsymbol{\nu}(f) = \Big(f(x_1), \dots, f(x_M)\Big), \tag{50}$$

where $x_1, ..., x_M \in \mathbb{T}$ are the sampling locations. The vectors $\mathbf{h}_k$ are then samples of the basis functions:

$$\mathbf{h}_k = \Big(\beta_{per,h}(x_1 - hk), \dots, \beta_{per,h}(x_M - hk)\Big) \tag{51}$$

From (33) and (34), we have:

$$\beta_{per,h}(x - nh) = \sum_{k\in\mathbb{Z}} \widehat{\beta}_h(2\pi k) e^{j2\pi k(x-nh)} \tag{52}$$

for $n = 0, \dots, N-1$. Hence, knowing the analytical expression for $\widehat{\beta}_h$, we can easily find the values $\beta_{per,h}(x - hk)$ by truncating the Fourier series, and finally, construct the measurements matrix $\mathbf{H}$.

2) Fourier sampling: In the case of Fourier sampling, we define the measurement operator as:

$$\begin{aligned}\boldsymbol{\nu}(f) = \Bigg(& \widehat{f}[0],\ \mathrm{Re}(\widehat{f}[1]),\ \mathrm{Im}(\widehat{f}[1]),\ \dots, \\ & \mathrm{Re}(\widehat{f}\left[\frac{M_{LF}}{2}\right]),\ \mathrm{Im}(\widehat{f}\left[\frac{M_{LF}}{2}\right]), \\ & \Big(\mathrm{Re}(\widehat{f}[k]),\ \mathrm{Im}(\widehat{f}[k])\Big)_{k\in\mathbf{HF}}\Bigg)\end{aligned} \tag{53}$$

where $\mathbf{HF}$ is a set of randomly chosen $M - M_{LF}$ high frequencies. In this way we are taking $M_{LF}+1$ low-frequency Fourier samples of the signal f (low-pass filter) and $M - M_{LF}$ high-frequency components. Notice that since $\widehat{f}[0]$ is a real number, we only take its real part, whereas the other samples $\widehat{f}[k]$, for $k \neq 0$, might have imaginary part as well. Note that the system matrix $\mathbf{H}$ is easily computed since coefficients of the Fourier series can be derived from (34).

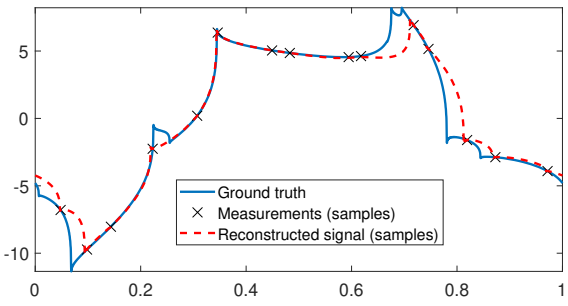

Figure 6: (γ, τ)-fractional periodic centered B-spline with $\gamma = 1.3$, $\tau = 0.3$. Sparsity: 20 after ADMM, 13 after Simplex. SNR = 13.57 dB.

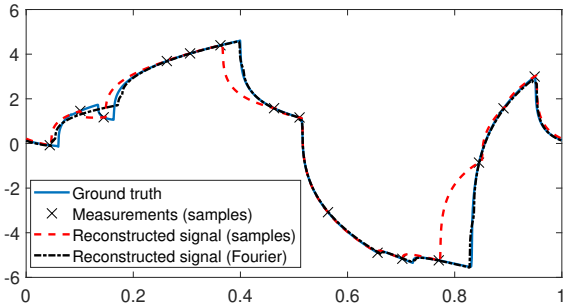

Figure 7: Reconstruction results for $\gamma = 1.3$, $\tau = \frac{\gamma}{2}$ fractional spline.
Ideal sampling$(- -)$: Sparsity = 14 after Simplex, SNR = 10.68 dB;
Fourier sampling$(- \cdot)$: Sparsity: 15 after Simplex, SNR = 26.93 dB.

B. Ground Truth Signal

In our experiments, we consider two types of ground truth signals: fractional L-splines and a SαS-processes.

1) Fractional Splines: The ground truth signal is of the form:

$$\mathrm{L}\{s\}(x) = \sum_{k=1}^{K_s} a_k \text{Ш}(x - x_k) \tag{54}$$

where K_s is the sparsity index, which can be chosen by the user, and the knots x_k are drawn from a uniform distribution in $\mathbb{T}$. Note that the knots x_k are not necessarily on the grid. Note that the ground truth signal is in the span of feasible signals that can be reconstructed using the discretized optimization problem if the approximation error on knot locations is ignored.

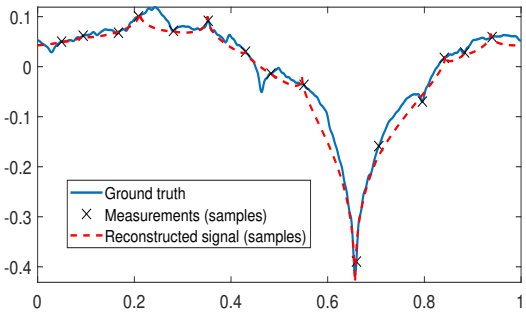

(a) gTV regularization (SNR = 14.65 dB)

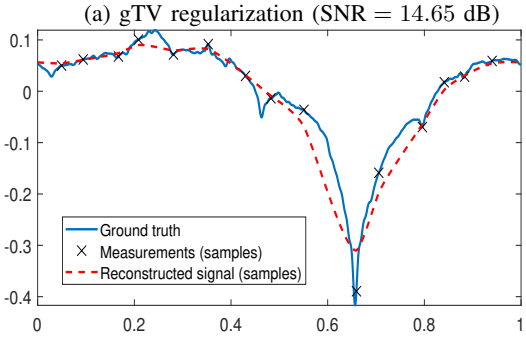

(b) L_2 regularization (SNR = 10.68 dB).

Figure 8: Reconstruction of a self-similar process (α = 1). Regularization operator $(\gamma, \tau) = (1.3, 0)$.

2) SαS-Processes: The notion of Gaussian bridge as a modification of the Brownian bridge has previously been explored in [20]. We generalize Brownian bridges for all SαS processes, with $\alpha \in (0, 2]$. The difference is in the innovation process w which is now a SαS-process.

We generate the samples $(w[k])_{1\leq|k|\leq N_{\text{coeff}}}$ of a SαS-process and find $2N_{\text{coeff}}$ samples of its DFT $W[k]$, where $N_{\text{coeff}} \in \mathbb{N}$ is the number of Fourier series coefficients used to approximate the infinite Fourier series. In order to get small approximation error, N_{coeff} should be sufficiently large. Then, we generate the signal s as a generalized Brownian bridge defined by:

$$s(x) = \sum_{1\leq|k|\leq N_{\text{coeff}}} \frac{W[k]}{\widehat{L}[k]} e_k(x), \qquad (55)$$

where $(\widehat{L}[k])_{1\leq|k|\leq N_{\text{coeff}}}$ is the truncated Fourier series of the operator L given by (20).

C. Comparison between gTV and L_2 Regularization

In order to evaluate the effectiveness of our proposed reconstruction scheme, we compare our gTV approach with Tikhonov L_2 regularization. Let $\mathcal{H}_{\text{L}}$ be a Hilbert space defined by:

$$\mathcal{H}_{\text{L}} = \left\{ f \in \mathcal{S}'(\mathbb{T}) : \text{L}\{f\} \in L_2(\mathbb{T}) \right\} \qquad (56)$$

Our L_2-regularized problem is defined as:

$$\min_{f\in\mathcal{H}_{\text{L}}} ||\boldsymbol{\nu}(f) - \mathbf{y}||_2^2 + \lambda ||\text{L}\{f\}||_{L_2}^2 , \qquad (57)$$

which we solve using the exact reconstruction scheme proposed in [20].

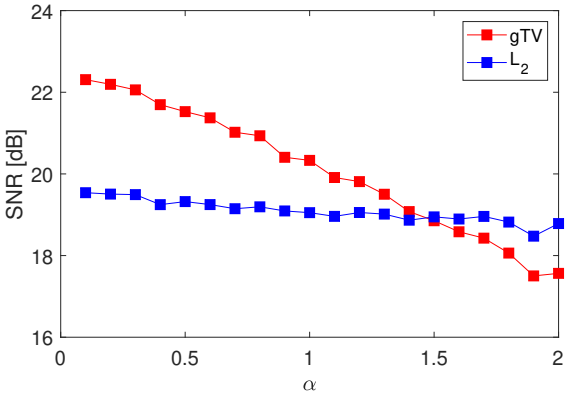

Figure 9: Comparison of gTV and L_2 regularization for different SαS-noises. The results are averaged over 500 realizations.

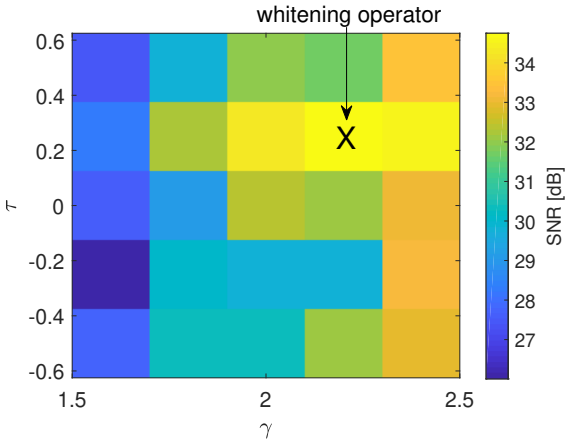

Figure 10: SNR values of the reconstruction for different regularization operators L_τ^γ. Whitening operator parameters: $\gamma_s = 2.2$, $\tau_s = 0.25$. The results are averaged over 20 realizations.

VIII. Experimental Results

Our algorithm is implemented using the GlobalBioIm library [40], developed at the Biomedical Imaging Group at EPFL.

A. Splines Reconstruction

In first set of experiments, we investigate the efficiency of reconstructing L-splines of the form (54) using our framework. To generate Figures 4, 5 and 6, we used the following settings: number of measurements $M = 15$, grid size $h = 2^{-7}$. For this and all experiments to follow, we choose the value of λ such as to maximize the SNR using grid search. The sparsity of the reconstructed signal after the simplex step was in the both cases smaller than the number of the measurements, which conforms with Theorem 1.

In Figure 7, we see the difference between ideal and Fourier sampling. From the Fourier series coefficients (34), we see that the spectrum of our signals decays as $|w|^{-\gamma}$. Therefore, the main part of spectrum of the signal is located at low frequencies.

Since with Fourier sampling we pick all the low-frequency components of the periodic signal, it is expected that this type of sampling produces better results, which is confirmed by the SNR values.

B. Self-Similar Processes

Some reconstruction of self-similar process with $\alpha = 1$ and ideal sampling is shown in Figure 8. Both the SNR values and plot show that gTV can reconstruct signals in a more accurate way than with L_2 regularization. This shows that gTV is more efficient in reconstructing sparse signals, even when the ground truth signal does not match the sparse spline model.
Due to the stochasticity of our framework, in the following sections we average our results over multiple realizations.

C. gTV vs L_2

In order to compare signal reconstruction using gTV and L_2 regularization, we vary the α parameter of the SαS-noise w from 0.1 to 2. We use a whitening operator L_s with parameters $\gamma = 1.5$ and $\tau = 0$, number of measurements $M = 30$, noise level SNR $= 20$ dB, grid size $h = 2^{-7}$ and Fourier sampling. The performance in terms of SNR are shown in Figure 9. As expected, lower values of α, indicating higher sparsity of the signal, result in better reconstruction using gTV regularization. On the other hand, L_2 performs better when the signal is not as sparse. Moreover, for the Gaussian case ($\alpha = 2$) L_2-regularized solution is a limit case of the MMSE and is practically optimal.

D. Whitening and regularization

In the following set of experiments, we investigate the correlation between the whitening operator L_s of the ground truth signal and the optimal regularization operator. The ground truth signal is a SαS-process with $\alpha = 1$. We take $M = 20$ ideal sampling measurements with noise level SNR $= 40$ dB. We use a whitening operator with parameters $\gamma = 2.2$, $\tau = 0.25$. The parameters of the regularization operator we used are $\tau = \{-0.5, -0.25, 0, 0.25, 0.5\}$ and $\gamma = \{1.6, 1.8, 2, 2.2, 2.4\}$. In Figure 10, we see that the maximum SNR is achieved when the regularization operator matches the whitening operator. Both γ and τ parameters influence the SNR of the reconstructed signal, which is not the case with L_2 regularization where the τ parameter has no influence on the reconstructed signal. This matching shows the pertinence of our model, since the best performance is achieved when the latter is respected.

E. Noise Influence

We investigate the influence of different noise levels. We use a SαS-process with $\alpha = 1$ as ground truth, and regularization operator L_τ^γ with $\gamma = 1.9$ and $\tau = 0$. As expected, lower noise results in higher SNR of the reconstructed signals for both gTV and L_2 regularization. Table I shows that gTV regularization is superior over L_2 independent of the noise level, which confirms that gTV regularization is better suited for sparse signals.

Measurement SNR [dB] (noise level)	SNR [dB] (gTV)	SNR [dB] (L_2)
20	21.13	20.80
40	28.62	27.79
60	29.28	28.76
no noise	29.30	28.94

Table I: Influence of the noise level on the reconstruction performance. The results are averaged over 100 realizations.

IX. Conclusion

In this paper, we have devised an algorithm for reconstructing periodic signals using variational methods with fractional derivative regularization. The periodic (γ, τ)-fractional B-splines were used as basis functions for the reconstructed signal. We have shown that the periodic setting enables us to discretize our continuous-domain optimization problem in an exact way. This results in a standard convex discrete optimization problem that can be solved.
As expected, Fourier-domain measurements yield solutions that are more accurate and have higher SNR in comparison with time-domain measurements.
We have also shown that this algorithm can be used for reconstructing self-similar processes of varying sparsity. We have shown that using gTV regularization can be more accurate in reconstructing sparse signals compared to L_2 regularization. The effects of varying parameters (γ, τ) of the regularization operator were examined and we have shown that the optimal regularization operator matches the whitening operator.

Appendix

A. Proof of Proposition 1

First, we prove that starting from the representation (38), we can determine the coefficients a_k, $k =$

$0, \dots, N-1$, from (37). Let $f = \sum_{k=0}^{N-1} c_k \beta_{per,h}(\cdot - kh)$. Then:

$$\begin{aligned}
\mathrm{L}\{f\}(x) &= \mathrm{L}\Big\{ \sum_{k=0}^{N-1} c_k \sum_{m\in\mathbb{Z}} \beta_h(x-kh-m) \Big\} \\
&= \frac{1}{h^{\gamma-1}} \sum_{k=0}^{N-1} c_k \sum_{m\in\mathbb{Z}} \sum_{l\in\mathbb{Z}} d[l]\delta(x-kh-m-lh) \\
&= \frac{1}{h^{\gamma-1}} \sum_{k=0}^{N-1} c_k \sum_{l\in\mathbb{Z}} d[l]\text{Ш}(x-(k+l)h) \\
&= \frac{1}{h^{\gamma-1}} \sum_{k=0}^{N-1} c_k \sum_{l\in\mathbb{Z}} d[l-k]\text{Ш}(x-lh) \\
&= \frac{1}{h^{\gamma-1}} \sum_{k,l=0}^{N-1} c_k d_{per}[l-k]\text{Ш}(x-lh) \\
&= \frac{1}{h^{\gamma-1}} \sum_{l=0}^{N-1} (\mathbf{c} * d_{per})_l \text{Ш}(x-lh) \qquad (58)
\end{aligned}$$

where $*$ is the discrete cyclic convolution operator defined as follows:

$$(\mathbf{c} * d_{per})_l = \sum_{k=0}^{N-1} c_k d_{per}[l-k] \ . \qquad (59)$$

Therefore, we conclude that f is of the form given in (37) with $a_k = \frac{1}{h^{\gamma-1}}(\mathbf{c} * d_{per})_k$, for $k = 0, \dots, N-1$.

Now we prove the reverse inclusion. Let $f \in \mathcal{M}_{\mathrm{L},h}(\mathbb{T})$, meaning that $\mathrm{L}\{f\} = \sum_{k=0}^{N-1} a_k \text{Ш}(\cdot - kh)$. Then, we have:

$$\begin{aligned}
\mathrm{L}\{f\}(x) &= \sum_{k=0}^{N-1} a_k \text{Ш}(x-kh) \\
&= \sum_{k=0}^{N-1} a_k \sum_{n\in\mathbb{Z}} e^{j2\pi(x-kh)n} \\
&= \sum_{n\in\mathbb{Z}} e^{j2\pi xn} \sum_{k=0}^{N-1} a_k e^{-j2\pi kn/N} \\
&= \sum_{n\in\mathbb{Z}} A[n] e^{j2\pi xn} \qquad (60)
\end{aligned}$$

using the Poisson summation formula.

By identification in (10), we conclude that:

$$\widehat{L}[n]\widehat{f}[n] = A[n] \qquad (61)$$

for all $n \in \mathbb{Z}$ and thus that $\widehat{f}[n] = \frac{A[n]}{\widehat{L}[n]}$ for $n \neq 0$ since $\widehat{L}[n] \neq 0$. Next, let $g = \sum_{k=0}^{N-1} c_k \beta_{per,h}(\cdot - kh)$. Then, g has Fourier series coefficients:

$$\begin{aligned}
\widehat{g}[n] &= \sum_{k=0}^{N-1} c_k \widehat{\beta}_{per,h}[n] e^{-j2\pi nkh} \\
&= \frac{1}{h^{\gamma-1}} \frac{\Delta_{per}[n]}{\widehat{L}[n]} \sum_{k=0}^{N-1} c_k e^{-j2\pi nkh} \\
&= \frac{1}{h^{\gamma-1}} \frac{\Delta_{per}[n]}{\widehat{L}[n]} C[n] \qquad (62)
\end{aligned}$$

for $n \neq 0$, and $\widehat{g}[0] = C[0]$. By identifying, we take $C[0] = \widehat{f}[0]$ and for $n \neq 0$:

$$C[n] = h^{\gamma-1} \frac{A[n]}{\Delta_{per}[n]} = A[n] V_{per}[n], \qquad (63)$$

where $V_{per}[n] = \frac{h^{\gamma-1}}{\Delta_{per}[n]}$ for $n \neq 0$, and $V_{per}[0] = 0$. Now, we can express $\mathbf{c}$ in time-domain as:

$$\mathbf{c} = \mathbf{a} * v + \widehat{f}[0]\mathbf{1} \qquad (64)$$

where v is the inverse DFT of V_{per}, and $\mathbf{1} \in \mathbb{R}^N$ is a vector of ones.

Then, f and g have identical Fourier series coefficients. This implies that $f = g$, which proves the desired result.

REFERENCES

[1] David L Donoho et al. Compressed sensing. *IEEE Transactions on information theory*, 52(4):1289–1306, 2006.

[2] Yonina C Eldar and Gitta Kutyniok. *Compressed sensing: theory and applications*. Cambridge university press, 2012.

[3] Ben Adcock and Anders C Hansen. Generalized sampling and infinite-dimensional compressed sensing. *Foundations of Computational Mathematics*, 16(5):1263–1323, 2016.

[4] Ben Adcock, Anders C Hansen, Clarice Poon, and Bogdan Roman. Breaking the coherence barrier: A new theory for compressed sensing. In *Forum of Mathematics, Sigma*, volume 5. Cambridge University Press, 2017.

[5] Benoit B Mandelbrot. *The fractal geometry of nature*, volume 173. WH freeman New York, 1983.

[6] Benoit B Mandelbrot and John W Van Ness. Fractional brownian motions, fractional noises and applications. *SIAM review*, 10(4):422–437, 1968.

[7] Jacques Levy-Vehel. Fractal approaches in signal processing. *Fractals*, 3(04):755–775, 1995.

[8] Stephen M Kogon and Dimitris G Manolakis. Signal modeling with self-similar/spl alpha/-stable processes: the fractional levy stable motion model. *IEEE Transactions on Signal Processing*, 44(4):1006–1010, 1996.

[9] Jacques Lévy Véhel. Introduction to the multifractal analysis of images, 1998.

[10] Beatrice Pesquet-Popescu and Jacques Lévy Véhel. Stochastic fractal models for image processing. 2002.

[11] Andras Eke, Peter Herman, J Bassingthwaighte, G Raymond, D Percival, Michael Cannon, Istvan Balla, and Cornelia Ikrényi. Physiological time series: distinguishing fractal noises from motions. *Pflügers Archiv*, 439(4):403–415, 2000.

[12] Ary L Goldberger, Luis AN Amaral, Jeffrey M Hausdorff, Plamen Ch Ivanov, C-K Peng, and H Eugene Stanley. Fractal dynamics in physiology: alterations with disease and aging. *Proceedings of the national academy of sciences*, 99(suppl 1):2466–2472, 2002.

[13] Marie Farge. Wavelet transforms and their applications to turbulence. *Annual review of fluid mechanics*, 24(1):395–458, 1992.

[14] Alberto Scotti, Charles Meneveau, and Seyed G Saddoughi. Fractal dimension of velocity signals in high-reynolds-number hydrodynamic turbulence. *Physical Review E*, 51(6):5594, 1995.

[15] Gregory W Wornell and Alan V Oppenheim. Estimation of fractal signals from noisy measurements using wavelets. *IEEE Transactions on signal processing*, 40(3):611–623, 1992.

[16] Thierry Blu and Michael Unser. The fractional spline wavelet transform: definition end implementation. In *2000 IEEE International Conference on Acoustics, Speech, and Signal Processing. Proceedings (Cat. No. 00CH37100)*, volume 1, pages 512–515. IEEE, 2000.

[17] Thierry Blu and Michael Unser. Self-similarity: Part ii—optimal estimation of fractal processes. *IEEE Transactions on Signal Processing*, 55(4):1364–1378, 2007.

[18] Michael Unser and Thierry Blu. Self-similarity: Part i—splines and operators. *IEEE Transactions on Signal Processing*, 55(4):1352–1363, 2007.

[19] Michael Unser and Pouya D Tafti. *An introduction to sparse stochastic processes*. Cambridge University Press, 2014.

[20] Anaïs Badoual, Julien Fageot, and Michael Unser. Periodic splines and gaussian processes for the resolution of linear inverse problems. *IEEE Transactions on Signal Processing*, 66(22):6047–6061, 2018.

[21] Grace Wahba. *Spline models for observational data*, volume 59. Siam, 1990.

[22] John Paul Ward, Julien Fageot, and Michael Unser. Compressibility of symmetric-α-stable processes. In *2015 International Conference on Sampling Theory and Applications (SampTA)*, pages 236–240. IEEE, 2015.

[23] SD Fisher and Joseph W Jerome. Spline solutions to l1 extremal problems in one and several variables. *Journal of Approximation Theory*, 13(1):73–83, 1975.

[24] Michael Unser, Julien Fageot, and John Paul Ward. Splines are universal solutions of linear inverse problems with generalized tv regularization. *SIAM Review*, 59(4):769–793, 2017.

[25] Julien Fageot and Michael Unser. Representer theorems for analog, periodic, and sparse signals.

[26] David L Donoho. Superresolution via sparsity constraints. *SIAM journal on mathematical analysis*, 23(5):1309–1331, 1992.

[27] Emmanuel J Candès and Carlos Fernandez-Granda. Super-resolution from noisy data. *Journal of Fourier Analysis and Applications*, 19(6):1229–1254, 2013.

[28] Kristian Bredies and Hanna Katriina Pikkarainen. Inverse problems in spaces of measures. *ESAIM: Control, Optimisation and Calculus of Variations*, 19(1):190–218, 2013.

[29] Vincent Duval and Gabriel Peyré. Sparse spikes deconvolution on thin grids. *arXiv preprint arXiv:1503.08577*, 2015.

[30] Quentin Denoyelle, Vincent Duval, and Gabriel Peyré. Support recovery for sparse super-resolution of positive measures. *Journal of Fourier Analysis and Applications*, 23(5):1153–1194, 2017.

[31] Axel Flinth and Pierre Weiss. Exact solutions of infinite dimensional total-variation regularized problems. *Information and Inference: A Journal of the IMA*, 8(3):407–443, 2018.

[32] Harshit Gupta, Julien Fageot, and Michael Unser. Continuous-domain solutions of linear inverse problems with tikhonov versus generalized tv regularization. *IEEE Transactions on Signal Processing*, 66(17):4670–4684, 2018.

[33] Thomas Debarre, Julien Fageot, Harshit Gupta, and Michael Unser. B-spline-based exact discretization of continuous-domain inverse problems with generalized tv regularization. *IEEE Transactions on Information Theory*, 2019.

[34] Mathews Jacob, Thierry Blu, and Michael Unser. Sampling of periodic signals: A quantitative error analysis. *IEEE Transactions on Signal Processing*, 50(5):1153–1159, 2002.

[35] Ricard Delgado-Gonzalo, Philippe Thévenaz, and Michael Unser. Exponential splines and minimal-support bases for curve representation. *Computer Aided Geometric Design*, 29(2):109–128, 2012.

[36] Thierry Blu and Michael Unser. A complete family of scaling functions: the (α, τ)-fractional splines. In *2003 IEEE International Conference on Acoustics, Speech, and Signal Processing, 2003. Proceedings.(ICASSP'03).*, volume 6, pages VI–421. IEEE, 2003.

[37] Michael Unser and Thierry Blu. Fractional splines and wavelets. *SIAM review*, 42(1):43–67, 2000.

[38] Stephen Boyd, Neal Parikh, Eric Chu, Borja Peleato, Jonathan Eckstein, et al. Distributed optimization and statistical learning via the alternating direction method of multipliers. *Foundations and Trends® in Machine learning*, 3(1):1–122, 2011.

[39] George B Dantzig, Alex Orden, Philip Wolfe, et al. The generalized simplex method for minimizing a linear form under linear inequality restraints. *Pacific Journal of Mathematics*, 5(2):183–195, 1955.

[40] E. Soubies, F. Soulez, M.T. McCann, T.-a. Pham, L. Donati, T. Debarre, D. Sage, and M. Unser. Pocket guide to solve inverse problems with GlobalBioIm. *Inverse Problems*, 35(10):1–20, October 2019. paper no. 104006.